ELSEVIER

Journal of Alloys and Compounds 404–406 (2005) 559–564

Journal of ALLOYS AND COMPOUNDS

www.elsevier.com/locate/jallcom

Process and mechanism of hydrogen-induced amorphization in C15 Laves phases RFe_2

K. Aoki[a,*], H.-W. Li[b], K. Ishikawa[a]

[a] *Department of Materials Science, Kitami Institute of Technology, 165 Koen-cho, Kitami, Hokkaido 090-8507, Japan*
[b] *Graduate School of Kitami Institute of Technology, Japan*

Received 8 September 2004; received in revised form 4 January 2005; accepted 11 January 2005
Available online 14 July 2005

Abstract

The pressure dependence of structural changes in C15 Laves phase $DyFe_2$ was investigated using a pressure differential scanning calorimeter (PDSC) at 0.1–5.0 MPa H_2 and compared with that of $ErFe_2$ and $CeFe_2$. By thermal analysis of $DyFe_2$, four exothermic peaks of hydrogen absorption, hydrogen-induced amorphization (HIA), the precipitation of BiF_3-type DyH_3 and the decomposition of the amorphous hydride were observed above 0.5 MPa H_2, although tri-hydride DyH_3 takes usually the HoH_3-type structure. HIA overlapped with the precipitation of DyH_3 at 0.2 MPa H_2, but *c*-$DyFe_2H_x$ decomposed directly into α-Fe and DyH_3 at 0.1 MPa H_2. Hydrogen absorption, HIA, and the decomposition of *a*-$DyFe_2H_x$ showed a negative pressure dependence, but the precipitation of DyH_3 showed a positive one. As a result of such dependence, HIA does not occur at lower hydrogen pressure. The structural changes of $ErFe_2$ were similar to that of $DyFe_2$. On the other hand, hydrogen absorption and HIA occurred simultaneously for every hydrogen pressure in $CeFe_2$. The mechanism of HIA in the C15 Laves phases RFe_2 was discussed on the basis of the experimental results.

Keywords: Hydrogen absorption; Transformation; Amorphous; Amorphization; Crystallization

1. Introduction

Since unique properties of amorphous alloys prepared by rapid quenching are lost by crystallization on heating, crystallization of amorphous alloys has extensively been investigated so far. On the other hand, it has been reported that some crystalline hydrides transform to amorphous ones on heating in a hydrogen atmosphere, which is called hydrogen-induced amorphization (HIA) and a reverse reaction to crystallization. HIA is closely related to the disproportionation reaction that dominates a lifetime of hydrogen storage alloys, so that it is important to make clear the controlling factors of HIA. HIA has been observed in the intermetallic compounds A_xB_{1-x} consisting of hydride forming (A) and non-hydride forming metals (B) with the crystal structures such as C15, $B8_2$, C23, $D0_{19}$ and $L1_2$ [1–15]. Among these, structural changes in the C15 Laves phases RFe_2 (R = rare earth metals) are particularly interesting, because both a crystalline and an amorphous hydride form depending on the hydrogenation temperature [12]. One of the present authors (Aoki) investigated hydrogen-induced structural changes in C15 Laves phases AB_2 and demonstrated that HIA occurs in the compounds having the atomic size ratio larger than 1.37 [16]. Recently, the present authors have shown that C14 Laves phase $NdMn_2$ with the atomic size ratio $R_{Nd}/R_{Mn} = 1.45$ amorphizes also by hydrogenation [17]. Furthermore, it has been reported that structural changes in C15 Laves phases RFe_2 depend on the kind of R [12,13]. That is, hydrogen absorption, HIA, the precipitation of RH_3 and the decomposition of the remaining amorphous phase occur in RFe_2 (R = Sm, Gd, Tb, Dy and Ho). On the contrary, hydrogen absorption and HIA occur simultaneously in $CeFe_2$ [18], while HIA and precipitation of ErH_3 do simultaneously in $ErFe_2$ [15]. However, the mechanism of HIA in the C15 Laves phases is still uncertain. It is important and useful to investigate formation conditions of

* Corresponding author. Tel.: +81 157 26 9452; fax: +81 157 26 9452.
E-mail address: aokiky@mail.kitami-it.ac.jp (K. Aoki).

0925-8388/$ – see front matter © 2005 Elsevier B.V. All rights reserved.
doi:10.1016/j.jallcom.2005.01.121

amorphous hydrides in order to elucidate the mechanism of HIA.

In the present work, the pressure dependence of structural changes in C15 Laves phase $DyFe_2$ is investigated using PDSC and compared with that of $ErFe_2$ and $CeFe_2$. The mechanism of HIA in the C 15 Laves phases RFe_2 is discussed on the basis of the experimental results.

2. Experimental

$DyFe_2$ was prepared using high purity metals by arc melting in a purified argon atmosphere and homogenized at 1073 K for 1 week in an evacuated quartz tube. After homogenization, the ingot was crushed into 100 mesh and thermally analyzed using a pressure differential scanning calorimeter (PDSC) in a hydrogen atmosphere of 0.1–5.0 MPa. The alloy was heated to typical stages in PDSC, followed by rapid cooling to room temperature. Subsequently, it was subjected to powder X-ray diffraction (XRD) and conventional DSC (Ar-DSC) heated at a rate of 0.67 K/s in a flowing argon atmosphere. Some samples were further examined in a transmission electron microscope (TEM). The thermal desorption spectrum (TDS) of hydrogen and the amount of desorbed hydrogen were measured by heating the sample at a rate of 2 K/s in an argon atmosphere by a hydrogen analyzer.

3. Results and discussion

3.1. Structural changes of $DyFe_2$ on hydrogenation and conditions of HIA

Fig. 1 shows typical PDSC curves of $DyFe_2$ and the change of the hydrogen content (H/M) heated at the rate of 0.17 K/s. The PDSC curves of $DyFe_2$ heated at 1.0, 0.2 and 0.1 MPa H_2 show four, three and two exothermic peaks, respectively.

Figs. 2 and 3 show XRD patterns and Ar-DSC curves of $DyFe_2$ heated to above the respective exothermic peaks at

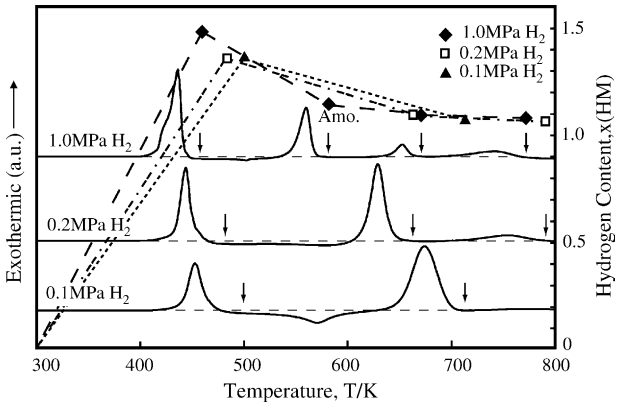

Fig. 1. PDSC curves of $DyFe_2$ and the change in the hydrogen content (H/M) heated at 0.1, 0.2 and 1.0 MPa H_2 at the rate of 0.17 K/s.

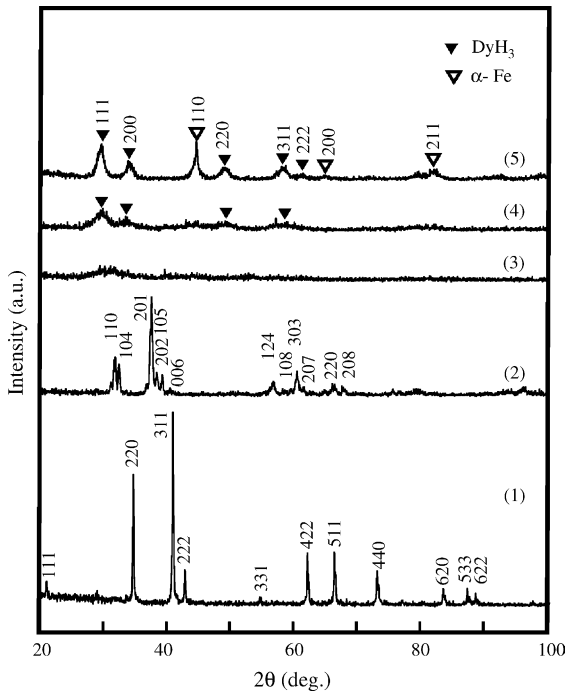

Fig. 2. XRD patterns of $DyFe_2$ heated to above the respective stages of PDSC at the rate of 0.17 K/s at 1.0 MPa H_2. The original sample (1), the sample heated to above the first peak (to 460 K) (2), the second peak (to 583 K) (3), the third peak (to 673 K) (4), and the fourth peak (to 773 K) (5).

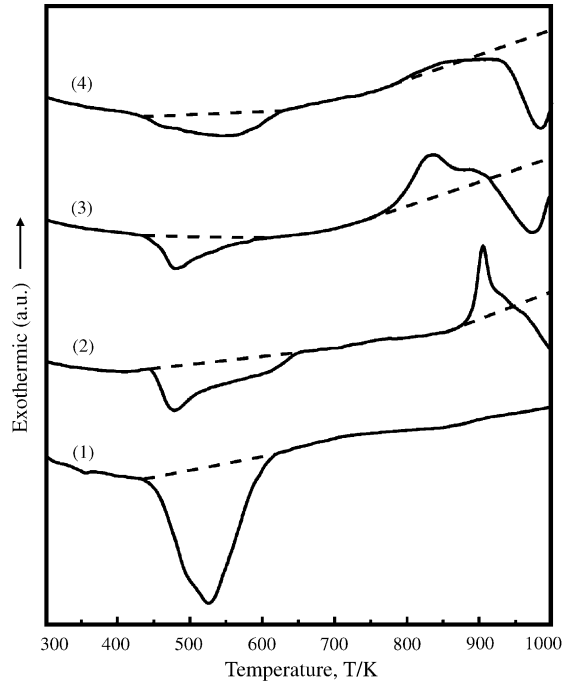

Fig. 3. Ar-DSC curves for $DyFe_2$ after heating to above the respective stages of PDSC at a rate of 0.17 K/s and at 1.0 MPa H_2. The sample heated to above the first peak (to 460 K) (1), the second peak (to 583 K) (2), the third peak (to 673 K) (3), and the fourth peak (to 773 K) (4).

1.0 MPa H_2, respectively. The XRD pattern of the original sample indicates that this alloy is in the C15 Laves phase. The XRD pattern of the sample heated to above peak I (to 460 K) shows Bragg peaks indexed on the basis of a rhombohedral structure ($R3m$). The bright field image (BFI) of TEM for this sample shows crystalline microstructure and the corresponding selected area diffraction pattern (SADP) shows a highly strained rhombohedral structure [20]. Its Ar-DSC curve does not show any exothermic peak of crystallization. Its hydrogen content is 1.48 (H/M). Consequently, the first exothermic peak results from the formation of a crystalline hydride c-$DyFe_2H_{4.4}$.

The Bragg peaks disappear and are replaced by a broad maximum in the sample heated to above peak II (to 583 K). BFI for this sample is featureless and its SADP shows a broad halo characteristic of the amorphous structure. The Ar-DSC curve of this sample shows an exothermic peak of crystallization at around 900 K. The hydrogen content is reduced to 1.13 (H/M). These experimental results imply that the second exothermic peak results from the transformation from c-$DyFe_2H_{4.4}$ to a-$DyFe_2H_{3.4}$, i.e., hydrogen-induced amorphization (HIA).

Broad and weak Bragg peaks of BiF_3-type DyH_3 appear overlapped with a broad maximum in the sample heated to above peak III (to 673 K). BFI shows crystalline particles embedded in the amorphous matrix and its SADP shows Debye–Scherrer rings of BiF_3-type DyH_3 overlapped with a broad halo. The Ar-DSC curve of this sample shows an exothermic peak of crystallization at around 800–900 K. From these experimental results, we can see that the third exothermic peak results from the precipitation of BiF_3-type DyH_3in a-$DyFe_2H_x$.

The XRD pattern of the sample heated to above peak IV (to 773 K) is indexed on the basis of α-Fe and BiF_3-type DyH_3. Dark particles can be observed in BFI for this sample and the Debye–Scherrer rings indexed on the basis of α-Fe and BiF_3-type $DyH_3$are observed in its SADP. Its Ar-DSC curve does not show any exothermic peak of crystallization. The hydrogen content of this sample is 1.08 (H/M), i.e., 3.24 (H/Dy). Consequently, the fourth exothermic peak results from the decomposition of the remaining amorphous hydride into α-Fe and DyH_3. The reaction sequence of $DyFe_2$ heated at 1.0 MPa H_2 is summarized as follows.

$$c\text{-}DyFe_2 \xrightarrow{\text{Peak I}} c\text{-}DyFe_2H_x \xrightarrow{\text{Peak II}} a\text{-}DyFe_2H_x \xrightarrow{\text{Peak III}} a\text{-}Dy_{1-y}Fe_2H_x + DyH_3 \xrightarrow{\text{Peak IV}} \alpha\text{-}Fe + DyH_3 \quad (1)$$

The PDSC curve of $DyFe_2$ heated at 0.2 MPa H_2 shows three exothermic peaks. The first and the third exothermic peaks result from hydrogen absorption and the decomposition of the a-$DyFe_2H_x$ into α-Fe and DyH_3, respectively, in the same way as 1.0 MPa H_2. On the other hand, the XRD pattern of the sample heated to above the second exothermic peak shows the Bragg peaks of BiF_3-type DyH_3 overlapped with a broad maximum. Its Ar-DSC curve shows the broad exothermic peak of crystallization. These experimental results imply that the second exothermic peak results from the simultaneous occurrence of HIA and the precipitation of BiF_3-type DyH_3. The reaction sequence of $DyFe_2$ heated at 0.2 MPa H_2 is expressed as follows.

$$c\text{-}DyFe_2 \xrightarrow{\text{Peak I}} c\text{-}DyFe_2H_x \xrightarrow{\text{Peak II}} a\text{-}Dy_{1-y}Fe_2H_x + DyH_3 \xrightarrow{\text{Peak III}} \alpha\text{-}Fe + DyH_3 \quad (2)$$

The PDSC curve of $DyFe_2$ heated at 0.1 MPa H_2 show two exothermic peaks. The first exothermic peak results from the formation of c-$DyFe_2H_x$. The XRD pattern of the sample heated to above peak II (to 714 K) is indexed on the basis of α-Fe and BiF_3-type DyH_3. BFI of this sample shows the lattice image and its SADP shows Debye–Scherrer rings indexed on the basis of α-Fe and BiF_3-type DyH_3. The Ar-DSC curve of this sample does not show any exothermic peak of crystallization. The hydrogen content of this sample is 1.36 (H/M), which is the same as that of the sample heated at 0.2 MPa H_2. Consequently, the second exothermic peak results from the direct decomposition of c-$DyFe_2H_{4.1}$ into α-Fe + DyH_3. No amorphous hydride is detected under the present experimental conditions. The reaction sequence of $DyFe_2$ heated at 0.1 MPa is expressed as follows.

$$c\text{-}DyFe_2 \xrightarrow{\text{Peak I}} c\text{-}DyFe_2H_x \xrightarrow{\text{Peak II}} \alpha\text{-}Fe + DyH_3 \quad (3)$$

Fig. 4 shows the relation between the peak temperatures T_p for the thermal reactions and the hydrogen pressure. T_p for hydrogen absorption, HIA, and the decomposition of the a-$DyFe_2H_x$ show a negative pressure dependence, but T_p for the precipitation of DyH_3 shows a positive one. Also, the extrapolated line connecting T_p for HIA intersects the extrapolated line connecting T_p for the precipitation of DyH_3. HIA and the precipitation of DyH_3 occur simultaneously at about 0.2 MPa H_2. At the hydrogen pressure below the intersecting point,

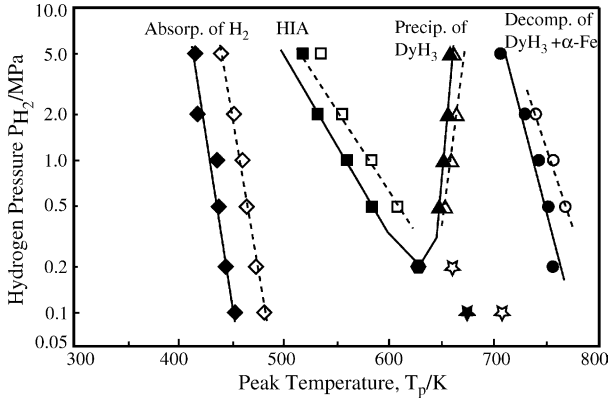

Fig. 4. The peak temperatures T_p of the thermal reactions of $DyFe_2$ for two heating rates of 0.17 K/s (the solid symbol and the solid line) and 0.33 K/s (the open symbol and the broken line) plotted against the hydrogen pressure. The solid hexagon denotes that HIA and the precipitation of BiF_3-type DyH_3 occur simultaneously. The pentagram indicates the direct decomposition of the crystalline hydride.

T_p for HIA is higher than that for the precipitation of DyH_3, which implies that a-$DyFe_2H_x$ is unstable. Then, c-$DyFe_2H_x$ decomposes directly into α-Fe and DyH_3at 0.1 MPa H_2. The reduced peak temperature (the peak temperature/the melting point of $DyFe_2$) T_p/T_m for hydrogen absorption, HIA, the precipitation of DyH_3 and the decomposition of a-$DyFe_2H_x$ are 0.28, 0.36, 0.43 and 0.48, respectively. These values are related with the diffusion of the metallic atoms as discussed later.

The relation between T_p and the hydrogen pressure for $ErFe_2$ is similar to that for $DyFe_2$ [19]. That is, T_p for hydrogen absorption, HIA and the decomposition of a-$ErFe_2H_x$ into α-Fe + ErH_3 show a negative pressure dependence, but T_p for the precipitation of BiF_3-ype ErH_3 shows a positive one. On the contrary, hydrogen absorption and HIA occur simultaneously in $CeFe_2$ independent of the hydrogen pressure [18]. T_p for HIA and the decomposition of a-$CeFe_2H_x$ show a negative pressure dependence, while T_p for the precipitation of CeH_3 shows a positive one. For every R, T_p for hydrogen absorption, HIA and the decomposition of a-RFe_2H_x show a negative pressure dependence, although hydrogen absorption and HIA occur simultaneously in $CeFe_2$, which implies that these reactions are controlled by the diffusion of hydrogen or R that interacts with hydrogen. On the contrary, T_p for the precipitation of BiF_3-type RH_3 shows a positive pressure dependence. This pressure dependence is very strange, because the increment of the hydrogen pressure usually enhances the diffusion of hydrogen. Thus, it is considered that the precipitation of BiF_3-type RH_3 is controlled by the diffusion of Fe that does not interact with hydrogen. In the work published on $CeFe_2H_x$ [18] and $ErFe_2H_x$ [19], the authors had attributed the respective PDSC peaks to the precipitation and the decomposition of Ce(Er)H_2 and not to that of Ce(Er)H_3. Now, in the present work, the authors interpret the corresponding peaks as due to the (cubic BiF_3-type) tri hydride DyH_3 on the basis of the hydrogen content. In the previous papers, the authors were misled in their interpretations, because they did not consider the hydrogen content of the hydrides. By reconsideration of it, the authors attribute the respective PDSC peaks to the precipitation and the decomposition of Ce(Er)H_3.

3.2. Structural changes on dehydrogenation

Fig. 5 shows TDS for the samples: (1) c-$DyFe_2H_{4.4}$, (2) a-$DyFe_2H_{3.4}$, (3) a-$Dy_{1-y}Fe_2H_x$ + DyH_3, (4) α-Fe + DyH_3 and (5) HoH_3 -type DyH_3 prepared by hydrogenation of Dy. TDS for c-$DyFe_2H_{4.4}$ shows sharp and overlapping peaks in the range 500–650 K, which indicates that all of the hydrogen is desorbed from this sample in the crystalline state. On the other hand, TDS for a-$DyFe_2H_{3.4}$ shows a small and sharp peak, at around 500 K, which is gradually weakened with increasing temperature. This peak indicates that some of hydrogen in a-$DyFe_2H_{3.4}$ is trapped in sites similar to those of c-$DyFe_2H_{4.4}$. The spectrum between 600 and 800 K (the shadowed part) implies that some of hydrogen atoms are

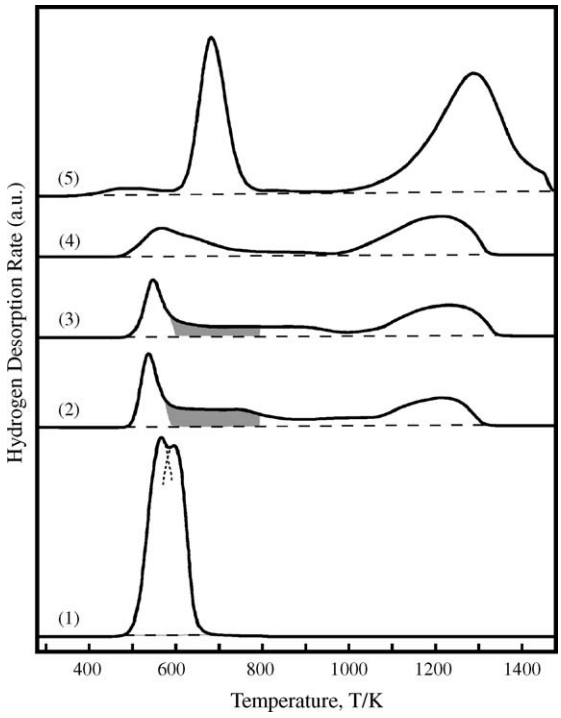

Fig. 5. TDS, heated at the rate of 2 K/s using a hydrogen analyzer in an argon atmosphere, for the samples: (1) c-$DyFe_2H_{4.4}$, (2) a-$DyFe_2H_{3.4}$, (3) a-$Dy_{1-y}Fe_2H_x$ + DyH_3, (4) α-Fe + DyH_3 and (5) for Dy hydride prepared by hydrogenation of Dy at room temperature in 5 MPa H_2 for 86 ks.

trapped more tightly than those in c-$DyFe_2H_{4.4}$, which becomes the driving force for HIA. On the other hand, TDS for this sample shows a broad peak at about 1100–1300 K, which is due to hydrogen desorption from CaF_2-type DyH_2. TDS for a-$Dy_{1-y}Fe_2H_x$ + DyH_3 is similar to that for a-$DyFe_2H_{3.3}$ because of the similarity of chemical compositions of both phases.

3.3. Crystal structures of R hydride precipitated in the amorphous hydride

Fig. 6 shows XRD patterns of (a) the Dy hydride (denoted by H) prepared by hydrogenation of Dy and subsequently heated to above the peaks of TDS and of (b) a mixture of α-Fe + Dy hydride (denoted by P) and subsequently heated to above the peaks of TDS. The hydrogen content (H/Dy) for these samples is shown in this figure. The XRD pattern of the Dy hydride (H) is indexed on the basis of HoH_3-type DyH_3. The XRD patterns of this sample heated to above the first peak (to 973 K) and to above the second peak (to 1773 K) of TDS are indexed on the basis of CaF_2-type DyH_2 and pure Dy, respectively. Consequently, the first and the second peak of TDS are due to the transformation from HoH_3-type DyH_3 to CaF_2-type DyH_2 and from CaF_2-type DyH_2 to pure Dy, respectively. On the contrary, the XRD pattern of the Dy hydride (P) does not change on heating to above the first peak of TDS (to 973 K). Since the hydrogen content decreases from 3.21 to 2.25 (H/Dy), the Dy hydride (P) and the heated

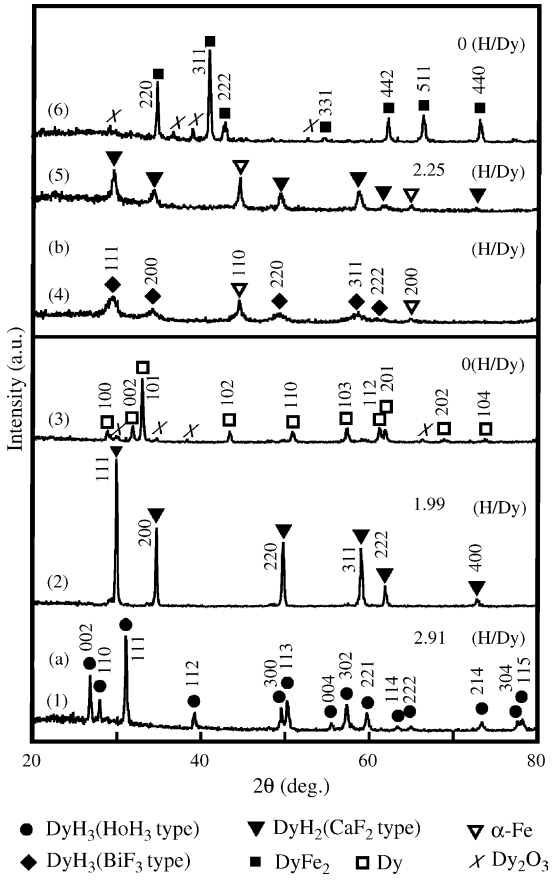

Fig. 6. XRD patterns of (a) Dy hydride prepared by hydrogenation (1) and subsequently heated to 973 K (2), and 1773 K (3) in the hydrogen analyzer and of (b) a mixture of α-Fe + DyH_3(4) prepared by hydrogenation of the amorphous alloy and subsequently heated to 973 K (5) and to 1373 K (6).

samples are considered to be BiF_3-type DyH_3 and CaF_2-type DyH_2, respectively. That is, the first and the second peak in TDS are due to the transformation from BiF_3-type DyH_3 to CaF_2-type DyH_2 and that from CaF_2-type DyH_2 to pure Dy, respectively.

Next, we discuss why HoH_3-type DyH_3 is not formed, but BiF_3-type DyH_3 is formed by the precipitation and by the decomposition of a-$DyFe_2H_x$. When CaF_2-type DyH_2 transforms into HoH_3-type DyH_3 by hydrogen absorption, large structural changes of the host metal Dy must occur. On the contrary, CaF_2-type DyH_2 transforms into BiF_3-type DyH_3 without a change in the crystal structure. CaF_2-type DyH_2 precipitated in a-$DyFe_2H_x$ is surrounded by the amorphous hydride, so that its transformation into HoH_3-type DyH_3 is hindered by it. Consequently, BiH_3-type DyH_3 may be formed by the precipitation in the amorphous hydride and the decomposition of the amorphous hydride.

3.4. The mechanism of hydrogen-induced amorphization (HIA) in C15 Laves RFe_2

We discuss the mechanism of HIA in $DyFe_2$ on the basis of the pressure dependence of structural changes. At 0.28 T_m, where no substantial diffusion of the metallic atoms occurs, hydrogen is absorbed forming c-$DyFe_2H_x$ without structural change. When c-$DyFe_2H_x$ is heated to above the second exothermic peak (to 583 K), i.e., to about 0.36 T_m, where both Dy and Fe atoms can move over a short-range distance, HIA occurs so as to reduce the enthalpy. The driving force for HIA in C15 Laves phases RFe_2 is considered to be the enthalpy difference resulting from the different hydrogen occupation sites.

The nearest neighbor coordination numbers of Fe and Tb atoms around the D atom, $N_{D\text{-}Fe}$, and $N_{D\text{-}Tb}$, calculated from the area under the Gaussian peaks in the RDF(r)s, together with the interatomic distance, r_1, for the Fe-D and Tb-D pair correlations, have been reported by us [21]. $N_{D\text{-}Fe}$ and $N_{D\text{-}Tb}$ for c-$TbFe_2D_{3.8}$ are nearly 2 and the total number of them is 4, which indicates that the D atoms occupy tetrahedral sites consisting of 2Fe + 2Tb. Three kinds of tetrahedral sites exist, i.e. 2R + 2Fe, 1R + 3Fe and 4Fe in the C15 Laves phases [22]. Table 1 clearly shows that only 2R + 2Fe site is occupied by the D atoms. In contrast, it has been predicted that five kinds of tetrahedral sites exist, 4R, 3R + 1Fe, 2R + 2Fe, 1R + 3Fe, and 4Fe in the corresponding amorphous a-RFe_2. Among these sites, D may occupy 4R, 3R + 1Fe, 2R + 2Fe sites because of the large formation enthalpy of the rare earth metal hydride. The occupation of these sites was confirmed by the neutron diffraction analysis as follows. $N_{D\text{-}Fe}$ and $N_{D\text{-}Tb}$ for a-$TbFe_2D_{3.0}$ is approximately 1 and 3, respectively, but the total number of them is still 4. These experimental results imply that the D atoms do not occupy only 3Tb + 1Fe tetrahedral sites, but occupy 4Tb, 3Tb + 1Fe, 2Tb + 2Fe sites in a-$TbFe_2D_x$. The reason is that if they occupy only 3Tb + 1Fe sites, $N_{D\text{-}Fe}$ and $N_{D\text{-}Tb}$ for a-$TbFe_2D_x$ must be independent of the D content. However, Table 1 shows that $N_{D\text{-}Fe}$ and $N_{D\text{-}Tb}$ for a-$TbFe_2D_x$ is reduced to 0.62 and increased to 3.3, respectively, by heating of a-$TbFe_2H_{3.0}$ at 473 K for 1 h in vacuum. This result indicates that the weakly trapped D atoms in 2Tb + 2Fe sites escape on heating. As a result, $N_{D\text{-}Fe}$

Table 1
Nearest neighbor coordination number, Ni_{i-j}, and interatomic distances, r_1, in c-$TbFe_2D_{3.8}$ and a-$TbFe_2D_x$ ($x = 3.0, 2.0$) calculated from the RDF(r)s observed by neutron diffraction

	D-Fe		D-Tb		Tb-Tb
	$N_{D\text{-}Fe}$ (atoms)	r_1 (nm)	$N_{D\text{-}Tb}$ (atoms)	r_1 (nm)	$N_{D\text{-}Fe} + N_{D\text{-}Tb}$ (atoms)
c-$TbFe_2D_{3.8}$	2.05	0.172	2.01	0.221	4.06
a-$TbFe_2D_{3.0}$	0.98	0.173	3.03	0.223	4.01
a-$TbFe_2D_{2.0}$	0.62	0.172	3.33	0.223	3.95

for a-$TbFe_2D_{2.0}$ is reduced, but $N_{D\text{-}Tb}$ for a-$TbFe_2D_{2.0}$ is increased. That is, D (or H) atoms in a-$TbFe_2D_x$ are much more strongly bound than those in the corresponding c-$TbFe_2D_x$. When c-$TbFe_2D_x$ is heated to the temperature where both Tb and Fe atoms can move over a short distance, at about 0.36 T_m, rearrangements can occur to reduce the total free energy of the system, which is HIA. BiF_3-type DyH_3 precipitates in the amorphous hydride at about 0.42 T_m. As the hydrogen pressure increases, the diffusion of hydrogen is generally enhanced which gives rise to a reduction of T_p. T_p for the precipitation of BiF_3-type DyH_3 shows positive (reverse) pressure dependence. Consequently, the precipitation of BiF_3-type DyH_3 may be controlled by the diffusion of Fe atoms that do not interact with hydrogen. The decomposition of the remaining amorphous hydride into α-Fe + DyH_3 is controlled by the long-range diffusion of both Fe and Dy atoms, because it occurs at 0.48 T_m where the long-range diffusion of them becomes generally more active.

The present work demonstrates that HIA in $DyFe_2$ and $ErFe_2$ occurs above a critical hydrogen pressure. We discuss the reason why HIA does not occur at low hydrogen pressure. The hydrogen content in c-$DyFe_2H_x$ is 1.48, 1.36 and 1.36 (H/M) for 1.0, 0.2 and 0.1 MPa H_2, respectively. Since there is little difference in the hydrogen content, it is considered that the occurrence of HIA is not determined by the hydrogen content, but by the hydrogen pressure. T_p for HIA shows a strong and negative pressure dependence, while that for the precipitation of BiF_3-type DyH_3 shows a weak and positive one. As a consequence of such pressure dependence, HIA overlaps with the precipitation of BiF_3-type DyH_3 at intermediate hydrogen pressure, while c-$DyFe_2H_x$ decomposes directly into α-Fe and BiF_3-type DyH_3 at low hydrogen pressure. Thus, the pressure dependence of HIA and the precipitation of BiF_3-type DyH_3 play an important role in determining whether HIA occurs or does not occur in $DyFe_2$. The pressure dependence of T_p for HIA may be controlled by short-range diffusion of the Dy and Fe atoms. On the other hand, it is a future subject to determine which atoms control the precipitation of BiH_3-type DyH_3.

4. Summary and conclusion

The pressure dependence of structural changes in the C15 Laves phase $DyFe_2$ heated in a hydrogen atmosphere between 0.1 and 5.0 MPa H_2 was investigated by PDSC, XRD, Ar-DSC, TEM and hydrogen analyzer and compared with that of $ErFe_2$ and $CeFe_2$. Four exothermic reactions, i.e., hydrogen absorption in the crystalline state, HIA, the precipitation of BiF_3-type DyH_3 and the decomposition of the remaining amorphous hydride occurred when $DyFe_2$ was heated at 0.5 MPa H_2. HIA and the precipitation of DyH_3 occurred simultaneously at 0.2 MPa H_2. The direct decomposition of the amorphous hydride into $DyH_3 + \alpha$-Fe occurred at 0.1 MPa H_2. As the hydrogen pressure increases, the peak temperature T_p for hydrogen absorption, HIA, and the decomposition of the amorphous hydride shifted to lower temperatures, but that for the precipitation of DyH_3 shifted slightly to higher temperature. That is, no amorphous hydride is formed at a low hydrogen pressure. The structural changes of $DyFe_2$ were similar to that of $ErFe_2$. On the other hand, hydrogen absorption and HIA occurred simultaneously in $CeFe_2$.The controlling factor for HIA in $DyFe_2$ was not the hydrogen content, but the hydrogen pressure that has a close relation with the diffusion of metal atoms. The driving force for HIA in C15 Laves phases RFe_2 was considered to be the enthalpy difference resulting from different hydrogen occupation sites as determined by neutron diffraction.

Acknowledgements

This work was supported in part by a “Grant-in-Aid” for Scientific Research on Priority Area a of “New Protium Function” from the Ministry of Education, Culture, Sports, Science and Technology.

References

[1] X.L. Yeh, K. Samwer, W.L. Johnson, Appl. Phys. Lett. 42 (1983) 242.
[2] K. Aoki, T. Yamamoto, T. Masumoto, Scr. Metal. 21 (1987) 27.
[3] L.E. Rehn, P.R. Okamoto, J. Pearson, R. Bhadra, M. Grimsditch, Phys. Rev. Lett. 59 (1987) 2987.
[4] U.-I. Chung, Y.-G. Lim, J.-Y. Lee, Phil. Mag. B 63 (1991) 1119.
[5] K. Aoki, T. Masumoto, J. Alloys Compd. 231 (1995) 20.
[6] A.Y. Yermakov, N.V. Mushnikov, N.K. Zajkov, V.S. Gaviko, V.A. Barinov, Phil. Mag. B 68 (1993) 883.
[7] K. Aoki, X.G. Li, T. Aihara, T. Masumoto, Mater. Sci. Eng. A 133 (1991) 316.
[8] S. Luo, J.D. Clewley, T.B. Flanagan, Acta Mater. 44 (1996) 4187.
[9] K. Aoki, Mater. Sci. Eng. A 304–306 (2001) 45.
[10] H. Atsumi, M. Hirscher, E.H. Buchler, J. Mossinger, H. Kronmüller, J. Alloys Compd. 231 (1995) 71.
[11] V. Paul-Boncour, S.M. Filipek, A. Percheron-Guegan, I. Marchuk, J. Pielaszek, J. Alloys Compd. 317–318 (2001) 83.
[12] M. Dilixiati, K. Kanda, K. Ishikawa, K. Aoki, Mater. Trans. 43 (2002) 1089.
[13] K. Aoki, K. Mori, T. Masumoto, Mater. Trans. 43 (2002) 2685.
[14] K. Aoki, M. Dilixiati, K. Ishikawa, J. Alloys Compd. 337 (2002) 128.
[15] K. Aoki, M. Dilixiati, K. Ishikawa, Mater. Sci Eng. A 375–377 (2004) 922.
[16] K. Aoki, X.-G. Li, T. Masumoto, Acta Metall. Mater. 40 (1992) 1717.
[17] K. Ishikawa, N. Ogasawara, K. Aoki, Phil. Mag. Lett. 84 (2004) 207.
[18] K. Aoki, M. Dilixiati, K. Ishikawa, J. Alloys Compd. 356–357 (2003) 664.
[19] K. Aoki, M. Dilixiati, K. Ishikawa, Mater. Sci. Eng. A 375–377 (2004) 922.
[20] H.-W. Li, K. Ishikawa, K. Aoki, J. Alloys Compd. 388 (2004) 49–58.
[21] K. Itoh, K. Kanda, K. Aoki, T. Fukunaga, J. Alloys Compd. 398 (2003) 167.
[22] D. Ivey, D. Northwood, J. Less-Common Met. 115 (1986) 23.